2A01

Fourier-transform spectroscopy of D_2^+ using intense near-infrared few-cycle laser pulses

○Toshiaki Ando, Atsushi Iwasaki, Kaoru Yamanouchi
Department of Chemistry, School of Science, The University of Tokyo, Japan

[Abstract] In order to obtain vibrational spectrum of D_2^+, we performed pump-probe measurements of D_2 by using intense near-infrared few-cycle laser pulses. The ion yields of D_2^+ and D^+ are recorded up to the pump-probe time delay of 527 ps. The ion yields oscillate as a function of the time delay and the oscillations reflect the motion of the vibrational wavepackets of D_2^+ created by the pump laser pulses. The vibrational level separations of D_2^+ are obtained with the uncertainties less than 0.01 cm^{-1} from the Fourier transform spectrum of the ion yields. The experimental vibrational level separations are in good agreement with the theoretically calculated values, showing a potential application of the strong-field pump-probe measurements to high-resolution spectroscopy of molecular cations.

[Introduction] Recent advances in ultrashort pulsed laser technologies have enabled us to generate few-cycle intense laser pulses and a vibrational wave packet of hydrogen molecular ions was probed in real time by using few-cycle intense laser pulses [1]. By monitoring the motion of the vibrational wave packet in the time domain, we can obtain the vibrational frequencies from the Fourier transform.

The vibration frequencies of hydrogen molecular ions have been determined by optical spectroscopy of molecular ions in an ion trap [2] and by PFI-ZEKE spectroscopy [3]. In the case of HD^+, the vibrational transition frequencies were determined with the precision of $\delta\nu/\nu = 10^{-9}$ by frequency-comb spectroscopy of HD^+ in a cold trap [2]. On the other hand, in the case of H_2^+ and D_2^+ having no dipole moment, the fundamental vibration frequencies were determined by PFI-ZEKE spectroscopy with an uncertainty of around 1 cm^{-1} [3].

In the present study, we determine the vibrational frequency of D_2^+ in the electronic ground $2\Sigma_g^+(1s\sigma_g)$ state with the uncertainties less than 0.01 cm^{-1} from the Fourier transform of the ion yields of D_2^+ and D^+ obtained by pump probe measurements using intense near-infrared few-cycle laser pulses.

[Methods] Linearly-polarized few-cycle intense laser pulses (5 fs, 780 nm) were generated by using a hollow-core fiber compression technique. The few-cycle laser pulses were introduced into a Mickelson interferometer to produce pump and probe laser pulses. The delay time between the two pulses, Δt, was scanned up to 527 ps by using an optical stage in the interferometer. The pump and probe pulses were focused onto an effusive molecular beam of D_2 in a time-of-flight mass spectrometer. The focal intensity was estimated to be 3.2×10^{14} W/cm^2. The ion yields of D_2^+ and D^+ were recorded as a function of Δt. The ion yields of D_2^+ and D^+ in the range of 370 fs < Δt < 527 ps are Fourier transformed.

[Results and Discussion] In the pump-probe measurement, the pump-pulse ionizes D_2 and prepares a vibrational wavepacket at the Franck-Condon region of the electronic ground $1s\sigma_g$ state of D_2^+, and then, the probe pulse creates light-dressed potential energy curves (PECs) as shown in Fig. 1(a), leading to the dissociation into $D + D^+$ through the three-photon crossing at R = 3.2 a.u. Because the vibrational wavepacket at the outer turning point of the PEC of the $1s\sigma_g$ state of D_2^+ dissociates through the three-photon crossing with a higher probability than the wavepacket at the inner turning point, the temporal variations in the yields of D_2^+ and D^+

should reflect the motion of the vibrational wavepacket. By Fourier transform of the delay time dependence of the difference in the ion yields of D_2^+ and D^+, we are able to obtain the FT spectrum in the frequency domain, from which we derive the vibrational level separations of D_2^+ as shown in Fig. 1(b).

In Table 1, the vibrational energy intervals, $\Delta G(v^+ + 1/2)$, obtained from the high-resolution FT spectrum are summarized, which agree well with the theoretical values whose accuracy is considered to be 1×10^{-4} cm^{-1} [4], showing that the strong field Fourier transform spectroscopy using few-cycle near-IR laser pulses is a promising method for the determination of vibrational level energies of molecular cations.

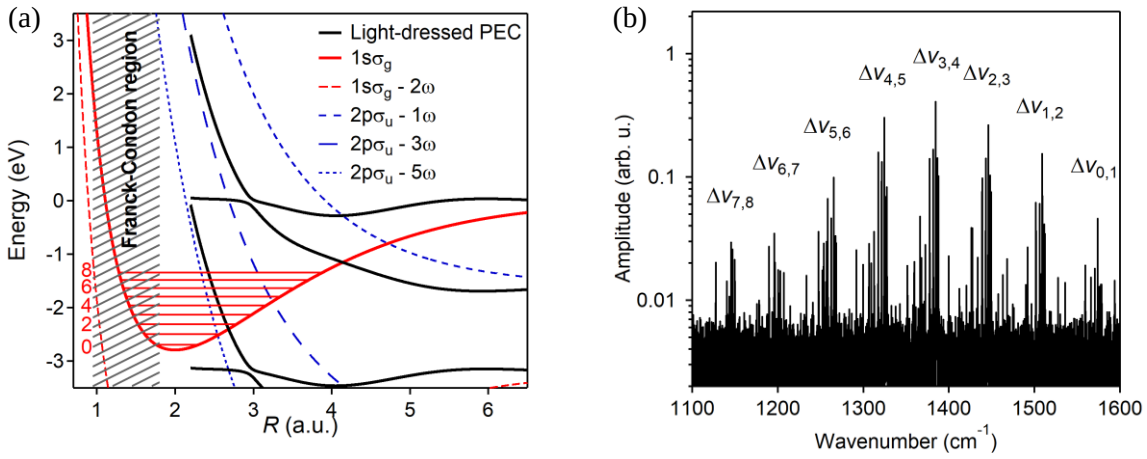

Figure 1. (a) The light-dressed PECs of D_2^+ interacting with a near-IR (775 nm) laser field at the laser field intensity of 3.2×10^{14} W/cm^2. The Fourier transform of the difference in the ion yields of D_2^+ and D^+ in the wave number range of 1100-1600 cm^{-1}.

Table 1. Comparison of the vibrational energy intervals (cm^{-1}), $\Delta G(v + 1/2)$, of D_2^+.

v	Present Experiment	Calculation [4]				Exp. - Calc.
		Non-adiabatic	Relativistic	Radiative	Total	
0	1577.0911(72)	1577.0706	0.0266	-0.0067	1577.0904	0.0007
1	1512.4033(19)	1512.3810	0.0245	-0.0063	1512.3993	0.0040
2	1449.3426(11)	1449.3261	0.0228	-0.0060	1449.3429	-0.0003
3	1387.7523(6)	1387.7365	0.0209	-0.0056	1387.7518	0.0005
4	1327.4621(9)	1327.4475	0.0193	-0.0053	1327.4614	0.0007
5	1268.3099(22)	1268.2975	0.0175	-0.0051	1268.3100	-0.0001

[References].

[1] T. Ergler et al., *Phys. Rev. Lett.* **97**, 193001 (2006).

[2] J. Biesheuvel et al., *Appl. Phys. B* **123**, 23 (2017).

[3] C. Chang et al., *Chin. J. Chem. Phys.* **20**, 352 (2007).

[4] R. E. Moss, *J. Chem. Soc., Faraday Trans.* **89**, 3851 (1993).

2A02

CEP dependences in single and double ionizations of methanol in intense few-cycle laser fields

Qiqi Zhang[1], Shinichi Fukahori[1], Toshiaki Ando[1], Reika Kanya[1], Atsushi Iwasaki[1], Tim Rathje[2], Gerhard G. Paulus[2], Kaoru Yamanouchi[1]

[1]*Department of Chemistry, School of Science, The University of Tokyo, Japan*

[2]*Institut für Optik und Quantenelektronik, Friedrich-Schiller-Universität, Jena, Germany*

[Abstract] The carrier-envelope-phase (CEP) dependences of single and double ionization processes in methanol were investigated by detecting the fragment ions by the coincidence momentum imaging (CMI) method. It was found that CH_3^+ generated from the dissociation of CH_3OH^+ is ejected mostly opposite to the direction of the electric field, indicating that the ionization rate is larger when the electric field points from the C atom to the O atom than when it points toward the opposite direction. On the other hand, CH_3^+ generated from the Coulomb explosion of CH_3OH^{2+} exhibits the phase shift of 0.7π with respect to CH_3^+ generated from the dissociation of CH_3OH^+. This phase shift suggests that the double ionization proceeds via the re-collision of the electron ejected through the tunnel ionization.

［**Introduction]** Recent developments of ultrafast laser technologies enable us to shorten a laser pulse so that the number of optical cycles within the pulse becomes only a few. Because the temporal shape of the electric field within the pulse varies depending on the carrier-envelope phase (CEP), responses of molecules to such few-cycle laser pulses are dependent on the CEP. Indeed, it has been revealed that the ionization and dissociation processes of molecules in a few-cycle laser field are influenced by the CEP [1]. Therefore, it is expected that, through the measurements of the CEP dependences, we will be able to deepen our understanding of complex mechanisms of molecular ionization and dissociation processes in an intense laser field. However, it is difficult to determine the absolute CEP at a spatial point where atoms and molecules interact with the few-cycle laser pulses because, in most cases, the CEP monitored in a separate apparatus have a constant offset with respect to the absolute CEP at the interaction point. Recently, Fukahori et al. [2] proposed an efficient method to determine an absolute CEP through the measurements of photoelectrons ejected from Ar by the irradiation of circularly polarized few-cycle laser pulses. In the present study, by adopting this method, we investigate the absolute CEP dependences in the single and double ionization processes of methanol by monitoring the asymmetry in the ejection direction of the fragment ions.

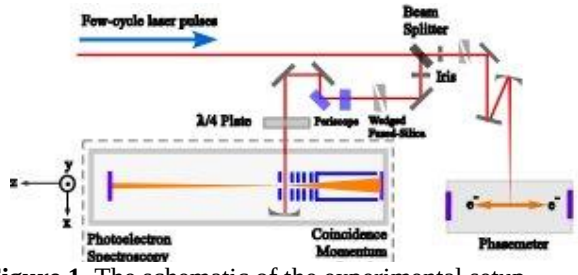

Figure 1. The schematic of the experimental setup.

[Methods] Figure 1 shows the experimental setup. Linearly polarized few-cycle laser pulses (4.5 fs, 760 nm, 5 kHz) were split into two by a beam splitter. One of the beams was introduced into a phasemeter [3] to record the CEP of each laser pulse, and the other was focused onto an effusive methanol beam in the vacuum chamber with which the CMI method are performed. The peak laser-field intensity at the laser-molecule interaction point was estimated to be 2.1×10^{14} W/cm^2, and the polarization direction of the laser pulse was parallel to the *y*-axis as shown in Fig. 1. The generated

fragment ions were accelerated by electrostatic lenses and were detected by a position sensitive detector. The three-dimensional momentum vectors of these ions were retrieved from their positions and the arrival times at the detector. The absolute CEP was calibrated by the CEP dependence of the photoelectrons generated from Ar in the circularly polarized few-cycle laser pulses.

[Results and discussion] The CEP dependences of the ejection direction of CH_3^+ produced from CH_3OH^+ ($CH_3OH^+ \rightarrow CH_3^+ + OH$) and from CH_3OH^{2+} ($CH_3OH^{2+} \rightarrow CH_3^+ + OH^+$) were investigated. The asymmetry parameter $A(\phi)$ describes the difference between the yields of CH_3^+ ejected upwards ($p_y > 0$) and downwards ($p_y < 0$) as a function of the CEP ϕ as

$$A(\phi) = \frac{N_{up}(\phi) - N_{down}(\phi)}{N_{up}(\phi) + N_{down}(\phi)}, \qquad (1)$$

where $N_{up}(\phi)$ and $N_{down}(\phi)$ denote the yields of the fragment ions ejected upwards and downwards, respectively. By a least-squares analysis, the ϕ dependence in the asymmetry parameter was fitted to a cosine function, $A(\phi) = A_0 \cos(\phi - \phi_0) + B$ where ϕ_0 denotes the CEP offset. Figure 2 shows the asymmetry parameters for the two decomposition channels producing CH_3^+. The CEP offsets were determined to be $\phi_0 = 1.13\pi$ and 1.85π for the decomposition channels from CH_3OH^+ and CH_3OH^{2+}, respectively.

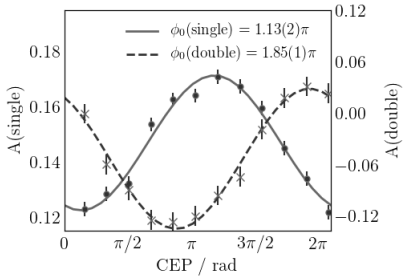

Figure 2. The CEP dependence of CH_3^+ generated from CH_3OH^+ and CH_3OH^{2+}. The black dots are the experimental data and the black lines are the best-fit asymmetry parameter, $A(\phi) = A_0\cos(\phi - \phi_0) + B$.

The CEP offsets value close to π for the decomposition channel from CH_3OH^+ shows that CH_3^+ ions are ejected preferentially toward the positive y direction at $\phi = \pi$. Figure 3(a) shows the electric field of the few-cycle laser field at $\phi = \pi$, and Fig. 3(b) shows the tunneling ionization rate w of methanol evaluated by the Ammosov-Delone-Krainov model [4]. The tunneling ionization rate becomes maxium at $t = 0$, at which the electric field is in the negative y direction, that is, the electric field is directed from the C atom to the O atom. Therefore, the tunneling ionization probability of methanol is larger when the electric field is directed from the C atom to the O atom than when the electric field direction is opposite.

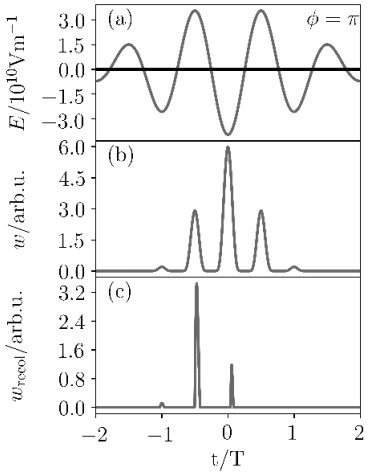

Figure 3. The results of the theoretical simulation when CEP = π (a) The electric field of the laser pulse. (b) The ionization rate of tunneling ionization. (c) The recollisional ionization rate w_{re}.

The recollisional ionization is known to contribute most to the double ionization of methanol by a few-cycle laser pulse [5]. Using the kinetic energies of a re-colliding electron obtained by solving the Newton's equation of motion, the recollisional ionization rate $w_{re}(t)$ was calculated as shown in Fig. 3(c) [1], showing that the recollsional ionization rate becomes maxium at $t = -0.47T$, where T is the period of optical cycles, at which the electric field is in the positive y direction, which is shifted by π compared with the tunneling ionization. This means that ϕ_0 of recollisional ionization is expected to be $\sim 2\pi$ ($= 0\pi$), which is in good agreement with the experimental value of $\phi_0 \sim 1.85\pi$. From the CEP dependences, we confirmed that the double ionization of methanol proceeds by the recollisional ionization.

[References]

[1] S. Miura *et al., Chem. Phys. Lett.* **595–596**, 61–66 (2014). [2] S. Fukahori *et al, Phys. Rev. A* **95**, 053410 (2017). [3] T. Wittmann *et al., Nat. Phys.* **5**, 357–362 (2009). [4] M. V. Ammosov *et al., Sov. Phys. JETP* **64**, 1191–1194 (1986). [5] R. Itakura *et al., J. Chem. Phys.* **127**, 104306 (2007).

2A03

原子価結合局在電子波束法による電子ダイナミクスの ポテンシャル面と高次高調波スペクトル

東京女子大・情報理学
○安藤耕司

Potential Energy Surfaces for Electron Dynamics and High-Harmonic Generation Spectra Computed with Localized Electron Wave Packets with Valence-Bond Spin Coupling

○Koji Ando
Department of Information and Sciences, Tokyo Woman's Christian University, Japan

【**Abstract**】A model of localized electron wave packets, floating and breathing Gaussians with non-orthogonal valence-bond spin-coupling, has been applied to construct potential energy surfaces for electron dynamics and to compute the high-harmonic generation (HHG) spectrum from a LiH molecule induced by an intense laser pulse. By computing the electronic energy of the model as a function of the wave packet center coordinates, the effective potential energy surfaces for the single electron motion are constructed. Numerically exact quantum dynamics are then computed on the effective potentials. The computed HHG spectra exhibited a plateau up to 50 harmonic order and a cut-off, in agreement with the previous time-dependent complete-active-space calculation despite the apparent and notable difference of the models. The present model thus offers a unique and unexpectedly rather simple picture of electron dynamics in chemical bond.

【**序**】近年の時間分解レーザー分光法は, アト秒オーダーの分解能を実現しており, 電子ダイナミクスを反映した信号の解析が可能となっている. 特に, 高強度レーザーパルスに誘起された高次高調波発生 (High-Harmonic Generation, HHG) 分光では, 分子から放出された電子がレーザー場の周期的変動に駆動されて元の分子に再衝突し, それがプローブとなって電子波動関数が検出されるという, いわゆる分子軌道トモグラフィーの可能性が検証されている. 理論計算では, 広い空間領域で高波数まで考慮する必要があるために, 原子軌道関数を基底とする従来法を単純に拡張したのでは不十分であり, 現実的な分子モデルによる量子ダイナミクス計算は未だ発展途上にある. 我々は, 波束中心を浮動させ, 波束幅も可変とする Gauss 型局在波束を基底とし, 非直交原子価結合理論によりスピン結合させた分子内電子モデルの可能性を探求している[1]. 昨年の本討論会では, LiH 分子について, 局在電子波束の準量子的ダイナミクス計算を報告した. HHG スペクトルの計算結果は, 約 100 次の高調波まで強度を持つ点は, 高精度計算 (Time-Dependent Complete Active Space, TD-CASSCF 法[2]) を再現したが, HHG スペクトルに特徴的な平坦領域やカットオフは再現されなかった[3]. これは, 単純な準量子的波束ダイナミクスでは量子干渉効果が適切に取り入れられていないためと推察し, 本研究ではそれを検証するために, 局在電子波束モデルを基にして電子運動のポテンシャルエネルギー曲面を構築し, その上で数値的に厳密な量子ダイナミクス計算を行った[4].

【**方法**】電子波動関数は, 空間座標関数とスピン関数の積を反対称化したものとし, 空間部分は Gauss 型波束の直積, スピン関数は Perfect-Pairing 型の単一配置とする. 個々の電子に対応する局在波束の運動を調べることで, 粒子的な描像も得られる. 理論の定式化を単純化するために, 多電子ダイナミクスを陽に扱う代りに, 着目する一電子の他の電子波束は固定して, それらの場の下での一電子ダイナミクスを考える. この場合, 時間依存変分原理により, 波束中心位置と幅について比較的単純な運動方程式が得られる. そのポテンシャルエネルギー関数は, 生のポテンシャルを波束で平均した有効ポテンシャルとなる. この運

動方程式のシミュレーションが,【序】で局在電子波束の準量子的ダイナミクス計算と記したもので, そのままでは波動関数の位相が適切に得られない. 位相を得るには, そのような局在波束ダイナミクスを多数走らせ, コヒーレント状態経路積分理論に基づいて作用関数に従った位相を与えモンテカルロ積分する[5]. しかし, LiH 分子の結合軸方向(Σ)および垂直方向(Π)励起のような低次元の問題であれば, 上記の有効ポテンシャル上での量子ダイナミクスを数値的に計算することも可能である. 今回はこれを実行することで, 一電子有効ポテンシャルを考察することの妥当性を検証する. それを受けて, より複雑な分子系にも適用可能なコヒーレント状態経路積分モンテカルロ法の実装に進む.

【結果】 Fig. 1 は, Li 2s と H 1s 電子に相当する波束に関する有効ポテンシャルのレーザー電場による変調を表す. これより, 以下が予測される: (i) H 1s 電子のポテンシャルには, 電場によるポテンシャルの変形により障壁が生じ, 電子は基本的に束縛されながら, トンネル効果によって外部へ滲み出る. (ii) Li 2s 電子のポテンシャルは浅いため, 電子はレーザー場の変調に直接的に追随する. このように, Fig. 1 のポテンシャルから定性的に示唆される描像は, 量子ダイナミクス計算で得られた座標期待値とその分散の計算結果から確認された. Fig. 2 は, 双極子期待値の加速度運動のフーリエ変換から計算した HHG スペクトルである. Li 2s 電子波束からのスペクトルが低次で強いことは, 上記のような場の変調に追随する運動から予測される. 50 次付近のカットオフへ至るプラトーは, H 1s 電子波束の寄与によることが見てとれる. このように Li 2s と H 1s 電子波束の寄与の単純和で高精度計算(TD-CASSCF 法[2])のスペクトルが再現されることは, 高強度場で誘起されたダイナミクスにおける両者の相関が小さいことを示唆する. 通常の分子軌道法では, LiH の σ 軌道において Li 2s と H 1s 原子軌道基底は強く混合しているが, 時間依存配置間相互作用ではこれらを分離するような配置間混合が動的に生じている可能性がある. その場合は複雑な配置間混合となると予想されるが, 一電子局在波束ダイナミクスを基底とする本モデルからは上記のように比較的単純な描像が得られる.

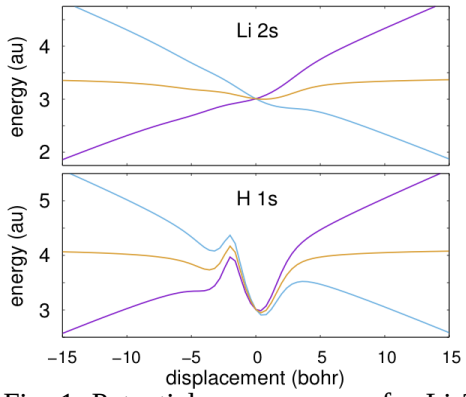

Fig. 1. Potential energy curves for Li 2s and H 1s electron wave packet centers modulated by the interaction with laser field at the peak intensities.

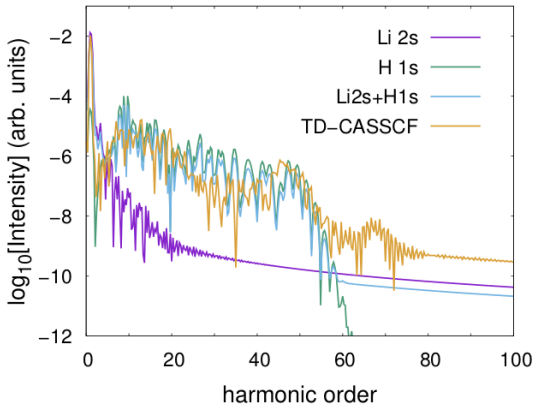

Fig. 2. High-harmonic generation spectra from the Fourier transform of dipole acceleration. The TD-CASSCF data is from Ref. [2].

【参考文献】

[1] K. Ando, *Bull. Chem. Soc. Jpn.* **82**, 975 (2009); *Chem. Phys. Lett.* **523**, 134 (2012); *J. Chem. Phys.* **144**, 12109 (2016).

[2] T. Sato and K. L. Ishikawa, *Phys. Rev. A* **91**, 023417 (2015).

[3] K. Ando, *Comp. Theor. Chem.* **1116**, 159 (2017).

[4] K. Ando, *J. Chem. Phys.* **148**, 094305 (2018).

[5] K. Ando, *Chem. Phys. Lett.* **591**, 179 (2014).

2A04

ICN分子のAバンド光解離反応における量子干渉効果

[1]慶大院理
○鹿志村達彦[1]，池崎智哉[1]，太田悠介[1]，藪下聡[1]

Quantum interference effect in the A-band photodissociation of ICN

○Tatsuhiko Kashimura[1], Tomoya Ikezaki[1], Yusuke Ohta[1], Satoshi Yabushita[1]
[1] Department of Chemistry, Keio University, Japan

【Abstract】

One of the most spectacular yet unsolved problems for ICN $\tilde{A}$-band photodissociation is the non-statistical spin-rotation F_1=N+1/2 and F_2=N-1/2 populations for each rotation level N of the CN fragment. The F_1/ F_2 population difference function $f(N)$ exhibits strong N and λ dependences with an oscillatory behavior. First, in the asymptotic region, we show that potential energy surfaces (PESs) are dominated by the exchange and dipole-quadrupole inter-fragment interactions. Then, we found that the adiabatic Hamiltonian exhibits Rosen-Zener-Demkov type nonadiabatic transitions reflecting the switch between the exchange interaction and the small but finite spin-rotation interaction within CN at the asymptotic region. Finally, we have derived semiclassical formulae for $f(N)$ and the orientation parameters with a two-state model including the 3A' and 4A' states. These two kinds of interfering models explain the F_1 and F_2 level populations observed by Zare's group and Hall's group, respectively.

【序】

ICN 分子の$\tilde{A}$バンド励起による光分解反応は、同種の光分解反応の中でも極めて詳細な情報が調べられてきた例である。実験的に、次の 2 つの解離チャネルが知られている。

$$\mathrm{ICN}+h\nu \rightarrow \begin{matrix} \mathrm{I}\left(^2P_{3/2}\right)+\mathrm{CN}(\mathrm{X}^2\Sigma^+,v,N,F_1/F_2) \\ \mathrm{I}^*\left(^2P_{1/2}\right)+\mathrm{CN}(\mathrm{X}^2\Sigma^+,v,N,F_1/F_2) \end{matrix}$$

ICN 分子は直線分子であるにも関わらず、生成物 CN は I チャネル、I*チャネルともに回転励起しており、かつそれらの回転準位 N の分布は I/I*チャネルに顕著に依存する。この N の分布や吸収断面積については理論計算によって再現がなされているが、CN 分子の回転微細構造準位 $F_1(J=N+1/2)/F_2(J=N-1/2)$の非統計的な振る舞い[2,3]に関しては未解決のままである。そこで、一光子によって同時に 3A'と 4A'のポテンシャルエネルギー曲面(PES)上に生じた解離波束間の量子干渉効果が、解離の漸近領域における角運動量の再結合による確率$p_{\mathrm{RZD}}=1/2$の RZD 型の非断熱遷移を通して、$f(N)$に反映されるとモデルを立てた(Fig. 1.)。[1]

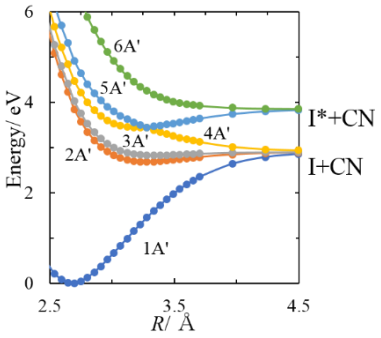

Fig. 1. PECs of a linear structure.[1]

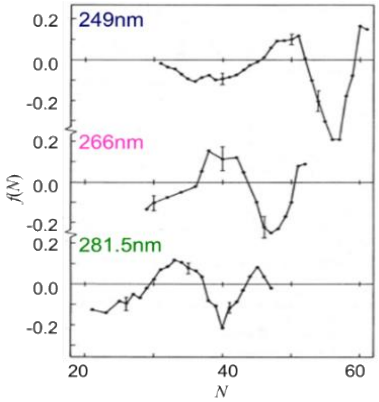

Fig. 2. $f(N)$.[2]

【理論】

Zare らによって、$\mathrm{CN}(X^2\Sigma^+,v=2,N,F_1/F_2)$が生じる場合の F_1/F_2分布 $P(F_1)/P(F_2)$の差の指標である$f(N)=[P(F_1)-P(F_2)]/[P(F_1)+P(F_2)]$が報告されている(Fig. 2.)。[2]この生成物はエネルギー保存則により I チャネルにのみ生成

するため、4A’と 5A’間の非断熱遷移は無視し、角運動量の再結合に起因する 3A’, 4A’間の RZD 型非断熱遷移のみを考慮する。始状態 i から光解離反応によって終状態 f を生成する断面積σ_fは半衝突散乱行列 S と遷移モーメント T を用いて$\sigma_f = \left|\sum_n S_{fn} T_{ni}\right|^2$であり、さらに半古典的散乱行列は$S = \mathrm{P}_\infty \mathrm{O}_{\mathrm{RZD}} \mathrm{P}_\mathrm{A}$と書ける。ここで P は伝搬行列であり断熱状態 n における位相ϕ_nを用いて$[\mathrm{P}_\mathrm{A}]_{nm} = \exp[i\phi_n]\delta_{nm}$である。還元散乱行列

$$\mathrm{O}_{\mathrm{RZD}} = \begin{bmatrix} \sqrt{1-p_{\mathrm{RZD}}} & -\sqrt{p_{\mathrm{RZD}}} \\ \sqrt{p_{\mathrm{RZD}}} & \sqrt{1-p_{\mathrm{RZD}}} \end{bmatrix} = \frac{1}{\sqrt{2}}\begin{bmatrix} 1 & -1 \\ 1 & 1 \end{bmatrix}$$

と遷移モーメント$\mathbf{T} = [t_{3A'} \quad t_{4A'}]$を代入することによって終状態の確率振幅を得る。

$$\begin{bmatrix} C(F_2) \\ C(F_1) \end{bmatrix} = \frac{1}{\sqrt{2}}\begin{bmatrix} 1 & -1 \\ 1 & 1 \end{bmatrix}\begin{bmatrix} e^{i\phi_{3A'}} & 0 \\ 0 & e^{i\phi_{4A'}} \end{bmatrix}\begin{bmatrix} t_{3A'} \\ t_{4A'} \end{bmatrix}$$

この結果を$P(F_1/F_2) = |C(F_1/F_2)|^2$に用いて$f(N)$の理論表式を得る。[1]

$$f(N) = \frac{P(F_1) - P(F_2)}{P(F_1) - P(F_2)} = \frac{2t_{3A'}t_{4A'}}{{t_{3A'}}^2 + {t_{4A'}}^2 + {t_{2A''}}^2 + {t_{4A''}}^2}\cos\Delta\phi$$

ただし$\Delta\phi = \phi_{3A'} - \phi_{4A'}$である。指標 $f(N)$は$\cos\Delta\phi$に依存することから 3A’と 4A’間の量子干渉効果が $f(N)$ に反映される。

【計算結果・考察】

ICN 分子の遷移モーメント(TDM)を Hellmann-Feynman (HF)型と応答量(Resp)型の二つの方法で計算したところよく一致する結果を得た(Figs. 3, 4)。過去の TDM の計算値[4, 5]は、今回の結果と振る舞いが異なる。さらに、CN を剛体回転子とみなし古典的軌跡$\{R(t), \theta(t)\}$に沿って、位相$\phi_{3A'}, \phi_{4A'}$を、次式の作用積分によって評価し、λ, N ごとにプロットしたところ

$$\phi_n(t + \Delta t) = \phi_n(t) + \sqrt{2M\left(E - V_n\left(R(t), \theta(t)\right) - BN(t)^2 - E_{\mathrm{vib}}\right)} \cdot \frac{P(t)}{M}\Delta t$$

定性的に Fig. 2 の指標 $f(N)$の振る舞いを再現することができた(Fig. 5.)。ここで M は I と CN の換算質量、E は励起エネルギー、V は PES、B とE_{vib}は、CN の回転定数と振動エネルギー、P は解離方向の運動量である。

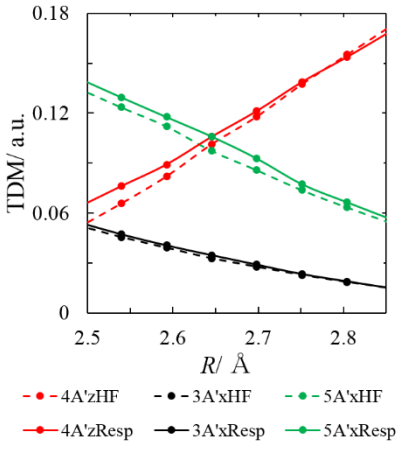

Fig. 3. R-dependence of TDM.

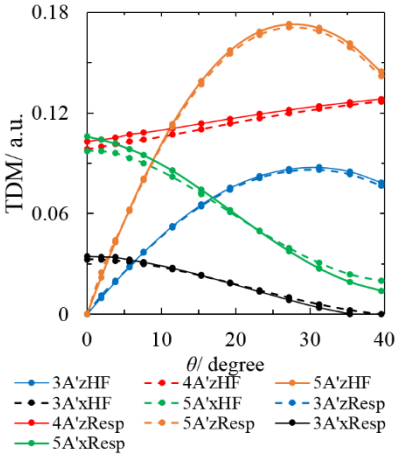

Fig. 4. θ-dependence of TDM.

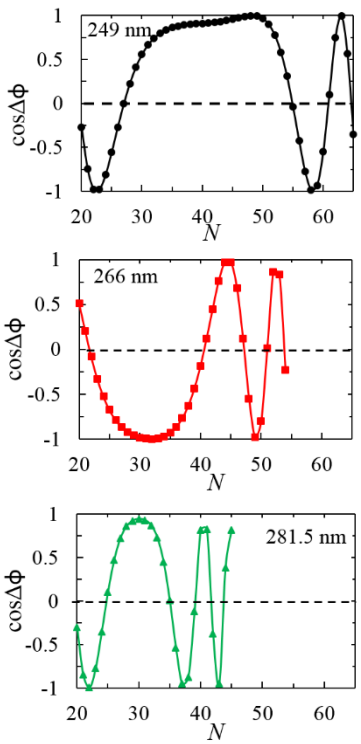

Fig. 5. $\cos\Delta\phi$.

【参考文献】

[1] T. Kashimura et al. *J. Comput. Chem.* submitted.[2] R. N. Zare, M. S. Child et al. *Faraday Discuss. Chem. Soc*. 1986, 82, 79. [3] G. E. Hall et al. *Phys. Chem. Chem. Phys.* 2007, 9, 272. [4] Y. Amatatsu et al. *J. Chem. Phys.* 1994, 100, 4894. [5] F. N. Dzegilenko et al. *Chem. Phys. Lett.* 1997, 264, 24.

2A05

Time-resolved photoelectron imaging using ultrashort VUV pulses

Takuya Horio*

Department of Chemistry, Graduate School of Science, Kyoto University, Japan

A photoexcited molecule is deactivated through a variety of photo-physical/chemical processes, and ultimately relaxes to the ground electronic state (S_0) or further undergoes chemical reactions in S_0. Time-resolved photoelectron imaging (TRPEI) [1] enables full observation of these photoinduced dynamics, because photoionization can be induced from any part of the potential energy surfaces (PESs). However, observation of low-lying electronic excited states and S_0 requires probe pulses in the vacuum ultraviolet (VUV) region, and it has been difficult to generate intense ultrashort VUV laser pulses.

Following the generation of sub-20 fs deep UV (DUV) pulses at 4.7 and 6.3 eV by cascaded filamentation four-wave mixing (FWM) [2], we have succeeded in generating ultrashort DUV and VUV (7.8 and 9.3 eV) pulses simultaneously [3,4]. While this light source is simple and easily implemented (Fig. 1), it provides multiple colors with ultrashort time-duration (<20 fs) without any dispersion control (Fig. 2). Thus, it is an ideal light for TRPEI. In this talk, we present TRPEI using ultrashort VUV pulses to obtain a "global reaction map" of photoinduced dynamics of an isolated molecule.

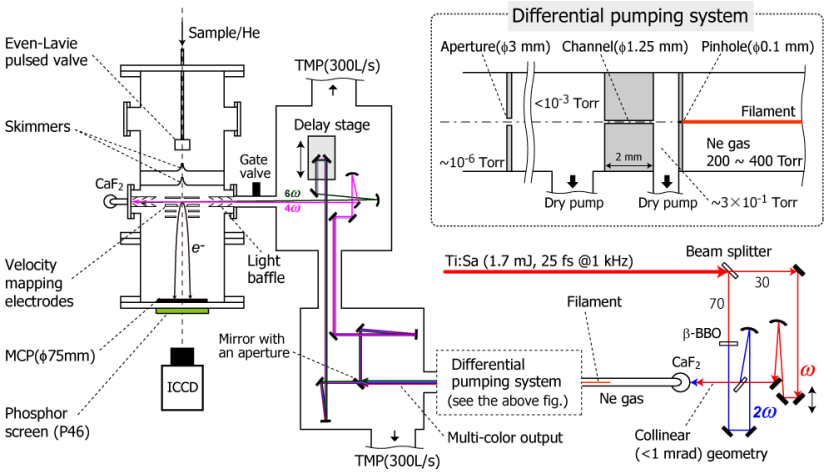

Figure 1. Schematic of the pump-probe photoelectron imaging system coupled with filamentation four-wave mixing light source.

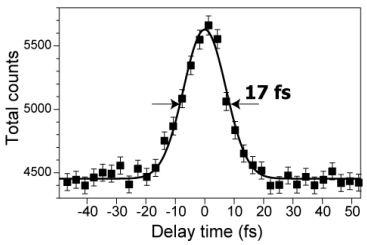

Figure 2. Cross-correlation trace between 6.3 and 9.3 eV pulses measured by non-resonant (1+1') two-photon ionization of Kr (squares). The solid line shows a Gaussian with a full width at half maximum of 17 fs.

The internal conversion (IC) from the $S_2(\pi\pi^*, {}^1B_{2u})$ state of pyrazine ($C_4H_4N_2$) to the $S_1(n\pi^*, {}^1B_{3u})$ state is one of the best-known example for ultrafast IC via conical intersection (CI) in PESs [5]. Since the S_2 Franck-Condon region is very close to the $S_2(\pi\pi^*)/S_1(n\pi^*)$ CI, IC occurs on an extremely short time scale (<30 fs). Using the sub-20-fs DUV pulses at 4.7 and 6.3 eV, respectively employed as pump and probe pulses, we successfully observed the $S_2(\pi\pi^*) \rightarrow S_1(n\pi^*)$ IC through time-dependent photoelectron angular distributions (PADs) [6]. It should be noted that the $S_1(n\pi^*)$ state of pyrazine populated from $S_2(\pi\pi^*)$ is also short lived and it undergoes further dynamics, which have not been fully elucidated due to insufficient

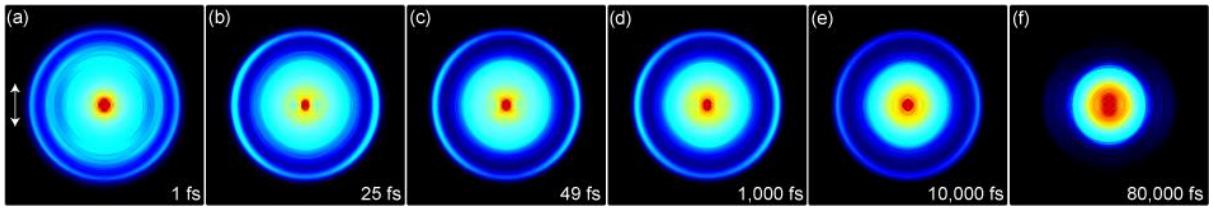

Figure 3. Photoelectron scattering distributions obtained at (a) 1, (b) 25, (c) 49, (d)1,000, (e)10,000, and (f) 80,000 fs. The directions of the polarization vectors of the 3ω and 6ω pulses are parallel to each other and vertical in the plane of the figure .

probe photon energy. Here we present full observation of the cascaded radiationless transitions from the $S_2(\pi\pi^*)$ pyrazine by TRPEI using the VUV probe pulses at 9.3 eV [7].

We excited jet-cooled pyrazine molecules into the $S_2(\pi\pi^*)$ state with 4.7–eV DUV pulses and probed subsequent electronic dephasing processes by single–photon ionization using 9.3–eV VUV pulses. Figures 3(a) – (c) present representative snapshots of the photoelectron scattering distributions observed at short time delays. The images observed at 1 and 25 fs are noticeably different, which manifests that the ultrafast $S_2(\pi\pi^*) \rightarrow S_1(n\pi^*)$ IC occurs on this ultrafast time scale. Figures 3(d) – (f) present representative snapshots of the photoelectron scattering distributions observed at long time delays. As seen in the figures, while the intensity of the outer ring, assigned as $D_0(n^{-1}) \leftarrow S_1(n\pi^*)$ photoionization signal, diminishes with the time delay, the inner part signals do not exhibit a noticeable decay within this time scale, indicating that long-lived state(s) are populated from $S_1(n\pi^*)$. We extracted time-dependent photoelectron spectra from the observed images and performed global fitting analysis to the spectra, which has revealed that the vibrationally-hot $S_1(n\pi^*)$ state further decays into S_0 and $T_1(n\pi^*)$ with a time constant of 14.8 ps. In this talk, we also demonstrate that the configuration interaction of the $S_2(\pi\pi^*)$ electronic wave function can be explored by ultrafast VUV photoionization (Figure 4). New experimental results on ultrafast electrocyclic ring-opening reaction are also presented.

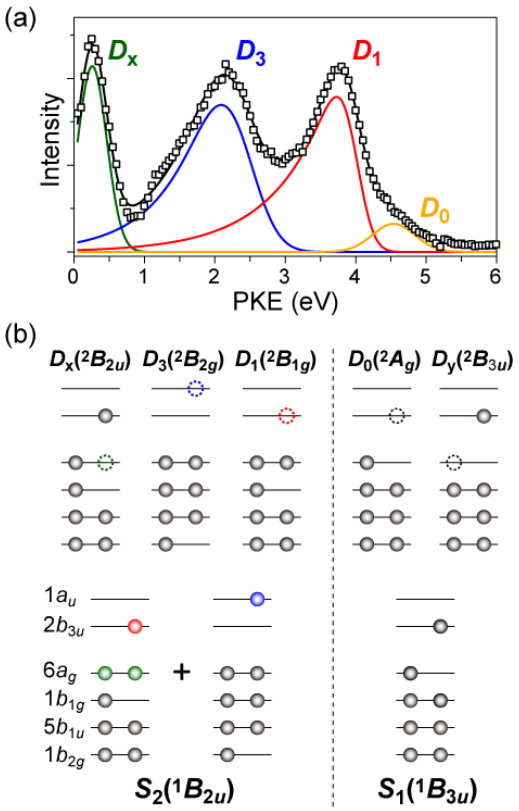

Figure 4. (a) Photoelectron spectrum of $S_2(\pi\pi^*)$. (b) The leading configurations for S_1, S_2, D_0, D_1, D_3, D_x, and D_y.

**Present address: Department of Chemistry, Graduate School of Science, Kyushu University, Japan*

【References】

[1] T. Suzuki, *Annu. Rev. Phys. Chem.* **57**, 555 (2006).
[2] T. Fuji, T. Horio, and T. Suzuki, *Opt. Lett.* **32**, 2481 (2007).
[3] T. Horio, R. Spesyvtsev, T. Suzuki, *Opt. Express* **21**, 22423 (2013).
[4] T. Horio, R. Spesyvtsev, T. Suzuki, *Opt. Lett.* **39**, 6021 (2014).
[5] W. Domcke et al., *Conical Intersections*, Vol. 15 of Adv. Ser. Phys. Chem.; World Scientific: Singapore, 2004.
[6] T. Horio, T. Fuji, Y.-I. Suzuki, and T. Suzuki, *J. Am. Chem. Soc.* **131**, 10392 (2009).
[7] T. Horio et al., *J. Chem. Phys.* **145**, 044306 (2016).

2A07

円錐交差の通過中および通過後の反応ダイナミクスを探る

[1]京大院理，[2]チューリッヒ工科大，[3]ヴュルツブルク大
○足立俊輔[1]，Tom Schatteburg[2]，Alexander Humeniuk[3]，Roland Mitrić[3]，鈴木俊法[1]

Probing ultrafast dynamics during and after passing through conical intersections

○S. Adachi[1], T. Schatteburg[2], A. Humeniuk[3], R. Mitrić[3], T. Suzuki[1]
[1] Department of Chemistry, Graduate School of Science, Kyoto University, Japan
[2] Laboratorium für Physikalische Chemie, ETH Zürich, Switzerland
[3] Institut für physikalische und theoretische Chemie, Julius-Maximilians-Universität Würzburg, Germany

【Abstract】 Introduction of vacuum-UV (VUV) probe pulses strengthens TRPES by enabling observation of ultrafast dynamics during and after passing through conical intersections (CIs). Here we present a VUV-TRPES study of furan, a prototypical heterocyclic molecule, using 14-eV probe pulses. Among two CIs involved in UV photochemistry of heterocyclic molecules, the ring-puckering CI plays a prominent role following the ππ* photoexcitation of furan. More than 90% of the excited molecules safely returns the original ground state, while the remaining 10% transforms into isomers after passing through the puckering CI.

【序】 比較的容易に得られる深紫外光($h\nu$ < 6 eV)をプローブとして用いた時間分解光電子分光(TRPES)では、Franck-Condon (FC)領域から円錐交差(CI)領域に至る励起状態での核波束運動や励起状態間の項間交差や内部転換の観測に限られる。しかし、TRPES のプローブとして真空紫外光(VUV)を用いれば、基底電子状態に至る CI の通過中あるいは通過後の反応ダイナミクスまでの全観測が可能になる [1–3]。本発表では、ヘテロ環分子の代表例であるフランの紫外光化学反応を VUV-TRPES により観測した結果について議論する。

ポンプ光($h\nu_{\mathrm{pump}}$ = 6.0 eV)によりフランを $^1B_2(\pi\pi^*)$電子状態に励起すると、(1) C–O–C 構造のパッカリング(面外変形)、(2) C–O 結合が切れる開環、の二通りの CI 構造を経由して分子は電子基底状態へと緩和する可能性がある(**Fig.1**)。しかし、どちらが主要な反応経路か、また反応生成物である異性体がどのような構造かに関しては、理論研究においても未だ議論が分かれている [4,5]。

【結果・考察】 TRPES において、観測量である光電子運動エネルギー(PKE)と、電子束縛エネルギー(eBE、分子から電子を取り去るのに要するエネルギー)との間には、$\mathrm{eBE} = h\nu_{\mathrm{probe}} - \mathrm{PKE}$なる関係がある($h\nu_{\mathrm{probe}}$：プローブの光子エネルギー)。CI 領域は FC 領域より低い電子エネルギーを持つため、一般に CI 領域への波束運動は eBE の増加を伴う。本研究でも、**Fig.2a** に示したように、スペクトルピークのシフトが励起後 150fs 以内に観測された。注目すべきは、τ ~ 90 fs (eBE ~ 5 eV)を境にしてスペクトルシフトの勾配が不連続になっていることである。これは、同時刻においてポテンシャルの勾配が突然変わったことを示唆し、この時刻に波束が CI を通過したと考えるのが最も妥当である。**Fig.2b** は、時間依存密度汎関数理論(TDDFT)に基づく量子ダイ

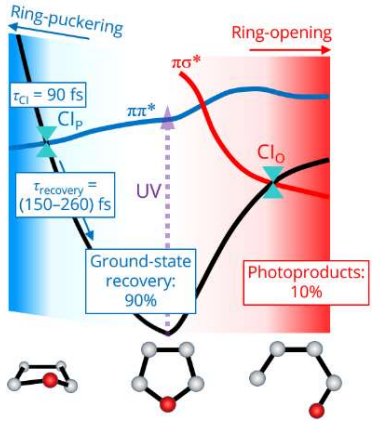

Fig. 1. Relaxation scheme of furan.

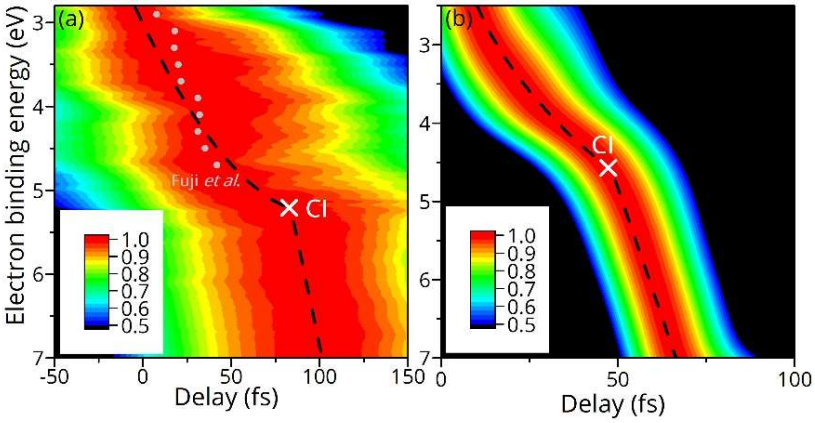

Fig. 2. Comparison between (a) experiment and (b) simulation.

ナミクス計算により得られた TRPES スペクトルであるが、スペクトルシフトの勾配が CI を境にして不連続になる様子が再現されている。我々のシミュレーションによると、ほぼ全ての反応トラジェクトリについて、基底状態への非断熱遷移はパッカリング CI を経由して進行する。またこの基底状態への非断熱遷移により、光励起で一時的に減少した基底状態ポピュレーションの回復(bleach recovery)が観測される(**Fig.3**、■)。この時間プロファイルに対するカーブフィッティングにより、bleach recovery が起こる時刻 $\tau_{recovery}$ = (150–260) fs と反応生成物の量子収率η = 0.09 が求められた。

以上、得られた結果を総合すると **Fig.1** のようになる。ππ*励起されたフランは、主にパッカリング CI を経由して電子基底状態へと緩和する。励起状態に生成された波束は τ_{CI} ~ 90 fs にパッカリング CI に到達し、引き続いて $\tau_{recovery}$ = (150–260) fs に電子基底状態に到達する。一連の緩和過程により、励起分子の 90%以上は元のフランの構造に戻る一方、残りの約 10%はパッカリング CI を通過後の後続反応により異性化する。当日の発表では、この反応生成物の分子種についても議論する予定である。

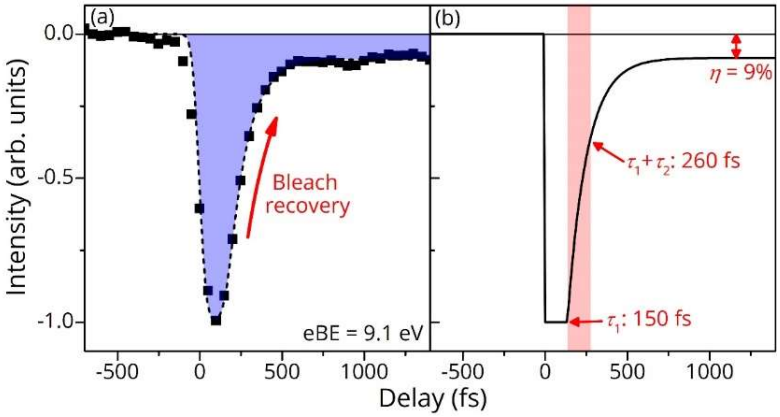

Fig. 3. (a) Time profile of photoelectron intensity at eBE = 9.1 eV (symbols) and the result of least-squares fitting (dashed curve). (b) Ground state dynamics determined from the fitting.

【参考文献】

1. S. Adachi, M. Sato, and T. Suzuki, J. Phys. Chem. Lett. **6**, 343 (2015).
2. T. Horio, R. Spesyvtsev, K. Nagashima, R. A. Ingle, Y. Suzuki, T. Horio, R. Spesyvtsev, K. Nagashima, and R. A. Ingle, J. Chem. Phys. **145**, 44306 (2016).
3. S. Adachi, H. Kohguchi, and T. Suzuki, J. Phys. Chem. Lett. **9**, 270 (2018).
4. T. Fuji, Y.-I. Suzuki, T. Horio, T. Suzuki, R. Mitrić, U. Werner, and V. Bonačić-Koutecký, J. Chem. Phys. **133**, 234303 (2010).
5. S. Oesterling, O. Schalk, T. Geng, R. D. Thomas, T. Hansson, and R. de Vivie-Riedle, Phys. Chem. Chem. Phys. **19**, 2025 (2017).

2A08

Calculation of absorption cross-sections and isotopic effects in photochemistry of S_2 and S_3

○Karolis Sarka[1,‡], Shinkoh Nanbu[1]
[1]*Department of Materials and Life Sciences, Sophia University, Japan*

Introduction

The photochemistry of elemental sulfur is one of the few unsolved questions in the photochemistry of atmospheres of late Archean period[1], Venus[2], Io[3], and other extraterrestrial atmospheres. It is prohibitively difficult to measure the spectra of fine-structure in ultraviolet due to the high temperature requirement for vaporization of elemental sulfur. For complete picture of the elemental sulfur photochemistry the photochemical cycle can be written down as: $S \longleftrightarrow S_2 \longleftrightarrow S_4 \longleftrightarrow S_8$; however, there are additional quasi-stable intermediate complexes present, thus we have to consider S_3, S_5, S_6, and S_7 compounds as well. Due to the number of degrees of freedom, at the present it is only possible to obtain exact solutions for S_2 and we are developing a solution for S_3. The sulfur dimer and trimer systems are isoelectronic to the oxygen and ozone cycle, and it is very likely that the sulfur undergoes a *Chapman mechanism*-like cycling in an anoxic atmosphere as well, reinforcing the isotopic fractionation occuring at each step.

To avoid the obstacles in experimental measurement, we turn to exact calculations of spectra based on time-independent Schrödinger equation, using R-matrix propagation of time-independent wavefunctions across the global potential energy curves for all discrete vibrational and rotational states and a combination of R-matrix and S-matrix for the continuum region.

Results and Discussion

We present the fine-structure spectra for sulfur dimer and its isotopologues as a sample of 1D system, including the precise source of mass-independent isotopic fractionation for compounds with low density-of-states. The potential energy curves and transition dipole moments are calculated at MRCI-F12/aug-cc-pVQZ level at full valence active space; absorption spectra are calculated for two lowest states with an allowed transition from the ground state ($X^3\Sigma_g^-$) – $B''^3\Pi_u$ and $B^3\Sigma_u^-$.

Based on the shifted fine-structure for each isotopologue, we have observed a strong excitation wavelength dependency for the mass-independent isotopic fractionation. It is clear that accurate evaluation of isotopic fingerprint for the atmospheric photochemistry of elemental sulfur needs a precise modeling setup, with spectral resolution approaching that of a natural broadening of a single absorption peak. The effects are also very susceptible to the shielding of competing absorbers and self-shielding. It is important to note that within a specific, narrow wavelength range, the molecule can exhibit both enriching and depleting isotopic effects, and this bimodal distribution of isotopic fractionation factor can be seen in three-isotope plot, Fig. 1. Strong dependency on specific wavelength of transition indicates that it is not acceptable to just assume a single value for a specific isotopologue – the evaluation must be performed carefully with a significant attention to detail.

‡E-mail to: ksarka@eagle.sophia.ac.jp

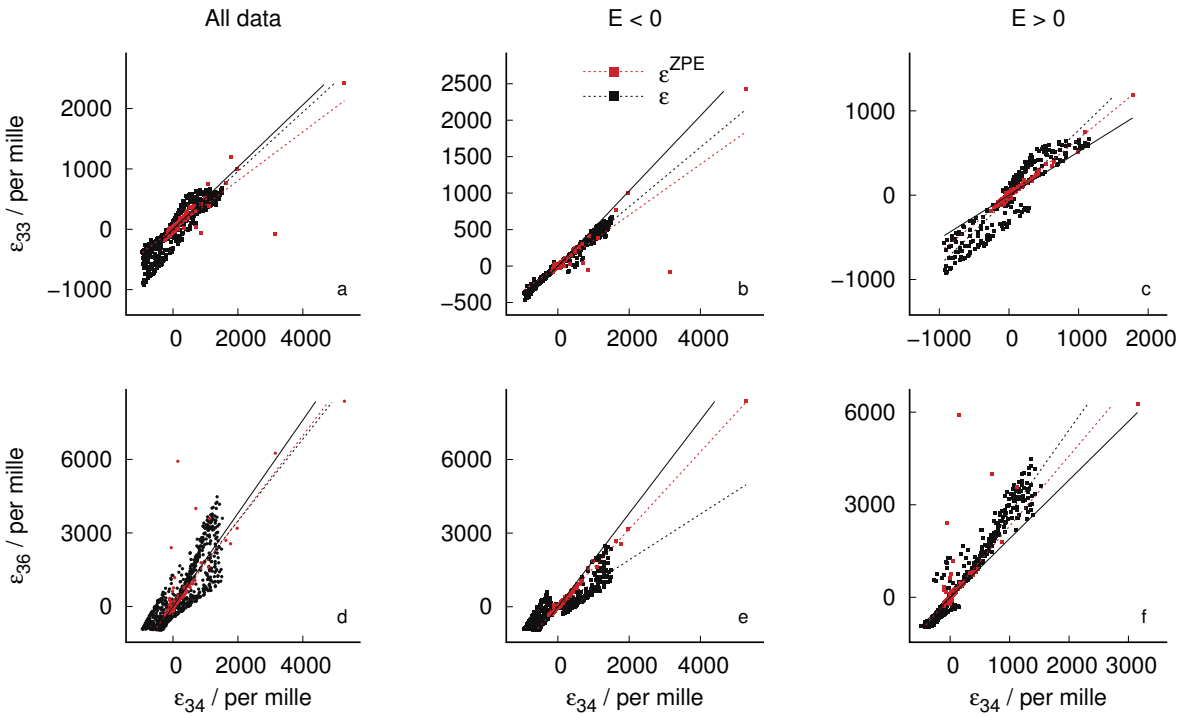

Figure 1: Three-isotope plots of $\varepsilon_{33}(\varepsilon_{34})$ (a-c) and $\varepsilon_{36}(\varepsilon_{34})$ (d-f). Solid lines represent MDF lines, dashed lines represent NLLS fit of the data. The data is split based on MIF factor E.

To evaluate the absorption cross-section of triatomic molecules we are developing a time-independent method based on proven theories of reactive scattering and ro-vibrational spectra calculation. The proposed mechanism is to solve the hyperspherical Schrödinger equation for each potential surface using a diabatic-by-sector approach, and to propagate the wavefunctions obtained at each sector over complete surface using the R-matrix theory. Once the wavefunctions and eigenergies are known, the remaining calculation of the absorption cross-section is trivial.

Conclusions

The spectra and mass-independent isotopic fractionation analysis indicate that sulfur dimer could play an important role in Archean earth and various extraterrestrial bodies. There is an ongoing search for unidentified absorbers and the spectral peak of S_2 lies precisely in the window that has few competing absorbers in an anoxic atmosphere. The feedback loop through S_3 is worth exploring and it might produce a significant isotopic fingerprint for elemental sulfur.

References

[1] James F. Kasting. The rise of atmospheric oxygen. *Science*, 293(5531):819–820, 2001.

[2] Xi Zhang, Mao Chang Liang, Franklin P. Mills, Denis A. Belyaev, and Yuk L. Yung. Sulfur chemistry in the middle atmosphere of venus. *Icarus*, 217(2):714 – 739, 2012. Advances in Venus Science.

[3] Kandis Lea Jessup, John Spencer, and Roger Yelle. Sulfur volcanism on io. *Icarus*, 192(1):24–40, 2007.